

# Experimental study of head shape effects on shear stress distribution around a single groyne

A. Safarzadeh, S.A.A. Salehi Neyshabouri & M. Ghodsian  
*Civil Engineering Department, Tarbiat Modares University, Tehran, Iran*

A. R. Zarrati  
*Civil and Environmental Engineering Department, Amirkabir University, Tehran, Iran*

**ABSTRACT:** Accurate experimental measurements were conducted to investigate the head shape effects on bed shear stress distribution around single straight and T-shape groynes. A yaw type Preston tube with 0.1 Pascal accuracy and 100 Hz sampling rate was used to locally measure the bed shear stresses in a non-uniform refined grid around a single groyne. The analysis of the results indicates a considerable difference in the bed shear stress distribution between the two types. The extension of the high shear stress zone is smaller in T-shape groynes, and its intensity decays much faster towards downstream. Flow visualization shows that in term of transverse oscillations, the separated shear layer downstream of the straight groyne is more stable, than the T-shape groyne. In addition, the distribution of shear stress is more uniform downstream of the T-shape groyne. In the straight type, the region of shear stress amplification was adjacent to the upstream part of the separated shear layer, whereas in T-shape case this region shifts toward the channel centreline. On the other hand, the maximum amplification of the bed shear stress (ratio of local bed shear stress to approaching flow shear stress) in T-shape groynes is about 35% smaller than for the straight one.

*Keywords: Groyne, T-Shape, Turbulence, Shear stress, Shear layer*

## 1 INTRODUCTION

Groynes or spur dikes are river training structures extending from the stream bank perpendicularly or with an angle to the watercourse. Groynes are used to: (1) deflect the high velocity flow away from river bank and control the bank erosion (2) increase sediment deposition near the river banks to improved channel alignment; (3) preserve the desired water depth, to improve the navigability of the river also to secure water supply (4) hydro environmental purposes such as restoring fish habitat and improving the river ecosystem.

Groynes may be built with different plan view shapes. Examples are straight groynes, T head, L head, hockey stick, inverted hockey stick, straight groyne with pier head and wing and tail groyne (Basak, 1999). Despite their useful features, construction of the groyne in river may cause some problems. When a groyne is placed in a channel, it causes a significant disturbance to the flow for a short distance upstream and for a longer distance downstream. Fig. 1 illustrates main features of turbulent flow around a single straight groyne in a fixed bed channel.

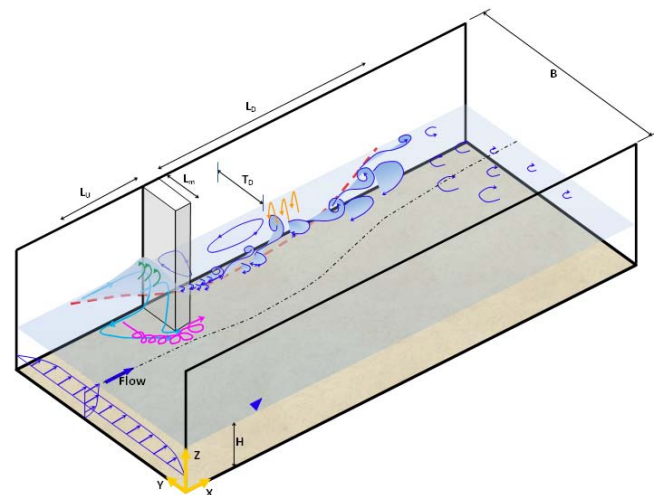


Figure 1. Main features of turbulent flow around a single straight groyne.

As the approach flow encounters a groyne it experiences a longitudinal pressure gradient, which cause separation of the flow from the channel side wall upstream of the groyne. This separation leads to the formation of a recirculation zone at this region. Strong down flow results from a stagnant vertical pressure gradient at the leading face of the groyne. Due to the down flow and the

adverse pressure gradient, the approaching bed boundary layer separates and a complex helically flow forms at the groyne base, known to the horseshoe vortex (HV).

Diverted flow at the groyne tip separates and a fully dynamic shear layer (SL) forms between the groyne wake (down stream recirculation region) and the main flow. The interface of separation zone and the main flow is an intense shear zone which downstream of the groyne becomes unstable and sheds vortices (Paik & Sotiropoulos, 2005).

The described phenomena cause a very complex 3D highly turbulent flow around the groyne. The HV system, the accelerated flow at the groyne tip, the down flow and the vortex shed inside SL locally induce large bed shear stresses and intensify near bed turbulence around the groyne. In alluvial rivers combinations of these factors cause the removal of bed materials and development of a local scour hole. Consequently the groyne may be undermined and fail.

Deflected flow at separate groyne tip along the shear layer, with high turbulent kinetic energy, picks up bed materials in its path and deposits them in locations of decreased velocity flow along the river bed further downstream. This kind of sedimentation is responsible for flooding due to an increase in channel resistance and reduces the flow depth locally. It is therefore important to recognize the shear stress zones or in another word the zones with high potential of scouring. Furthermore, the quantification of the maximum shear stress around groynes is important in sizing the riprap material used to prevent scouring at the groyne foundation. In this paper, straight and T shape groynes are used to investigate the effect of head shape on distribution of bed shear stresses around a single groyne over a smooth fixed flat bed. The main scope of this paper is to analyze the effect of the additional part (wing of the T shape groyne) on controlling the horseshoe vortex and shear stress amplification (ratio of local bed shear stress to approaching flow shear stress) at the groyne tip.

## 2 LITERATURE REVIEW

Knowledge on the bed shear stress distribution around groynes is based on a few past laboratory experiments and numerical studies. Awazu(1967) estimated the values of the bed shear stress around spur dikes using gradually varied flow equations and represented an equation for bed shear stress amplification. Zaghlol (1974) related the bed shear stress around the groyne to local velocity, vorticity and turbulence. Rajaratnam & Nwa-

chukwu (1983) measured bed shear stress experimentally around groyne like structures using a Preston tube for different protrusion ratios and Froude numbers. They found that the bed shear stress is amplified up to 5 times of the undisturbed approach shear.

Tingschali & Maheswaran (1990) used 2D shallow water equations with modified k- $\epsilon$  turbulence model to predict the flow field around groyne structures. They used the drag method (with a correction for 3D flow around groyne tip) to calculate the local bed shear stresses. Molinas et al. (1998) experimentally measured bed shear stresses around wall abutments using Preston tubes. The maximum shear stress was found to occur at the upstream corner of the abutment tip. The shear stresses around wall abutment were amplified up to 10 times and velocities were increased up to 50% depending up on flow conditions and abutment protrusion ratios. Ahmed & Rajaratnam (2000) measured the flow field and bed shear stress around a trapezoidal bridge abutment using a yaw probe. They found that the peak stress amplification of 3.63 occurs near the upstream corner of the abutment.

Teruzzi et al. (2009) employed LES model to analyze flow around a bridge abutment, and found that the calculated maximum value of the shear stress was nearly 13 times the approach flow shear, which was however confined in a very thin region near the upstream edge of the abutment. This simulation was in agreement with Ahmed & Rajaratnam (2000) who measured shear stress at bridge abutments with a Yaw probe. Recently some researchers measured the near bed turbulent Reynolds stresses using Acoustic Doppler Velocimeter (ADV) to estimate the local bed shear stress;  $\tau_b$ . Dey & Barbhuiya (2005) used this method to estimate the bed shear stress distribution in a scour hole at a semicircular abutment. Fazli et al. (2007) and Vaghefi & Ghodsian (2008) used the same method to calculate the bed shear stress around straight and T shape groynes in a movable bed 90 degree curved channel respectively. Duan (2009) and Duan et al. (2009) measured turbulent flow around a single spur dike in flat and scour beds respectively using ADV. In Duan's experiments the first measurement point was 1cm away from the streambed. The main drawback of this method is the inaccuracy of ADV measurements near the bed. Dombroski & Crimaldi (2007) found that Reynolds-stresses measured by an ADV agree with LDV measurement for distances more than 1 or 2 cm from the bed. In closer distances Reynolds stresses are under predicted by ADV. Precht et al. (2006) used synchronous ADV and LDA measurement to evaluate the near bed performance of the ADV in alluvial bed channels and

they found that for a distance about 2 cm from the bed, the velocities determined with ADV were at least 20% lower than those given by LDA and inaccuracy in turbulence characteristics may be much more.

Though recent experiments and especially numerical simulations have led to a much better understanding of the effects of turbulent flow on bed shear stress distributions around straight groynes and abutments, effect of groyne head geometry on flow field and associated shear stresses and scouring processes are still not well understood.

### 3 EXPERIMENTAL EQUIPMENTS AND PROCEDURE

#### 3.1 Laboratory facility

The laboratory experiments were conducted in a straight rectangular flume, 11m long and 1m wide, located at the hydraulic laboratory, Tarbiat Modares University. Fig. 2 shows the details of the flume. The channel side walls were from glass and the bed was made from 2cm thick smooth Perspex. Water in the flume was supplied by a pump. At the down stream end of the flume a fully automated flap weir was installed to regulate the depth of the flow. Small surface waves at the entrance of the flume were eliminated with the use of 1.5m long by 0.95m wide polystyrene plate held parallel to the upper water surface just down stream of the intake. The flow rate was controlled with a gate valve and was measured by means of a magnetic flow meter with an accuracy of 0.2%. Water surface profiles were measured with a digital point gauge with an accuracy of 0.01 mm.

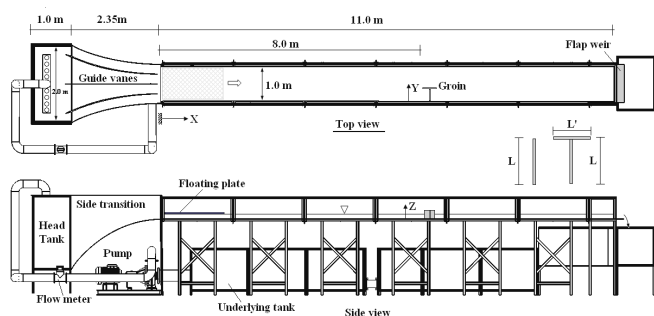


Figure 2. Details of the laboratory flume and groynes.

#### 3.2 Measurement instruments

Two different instruments were used during measurements. The first device was the vectorino type 10MHZ down looking ADV (Nortek) with an accuracy of 0.5% measured value, capable of measuring point-wise instantaneous 3D velocity field. A fully automated traversing system was designed

for positioning the ADV in position with accuracy of 0.1mm. The measured time series were filtered using the velocity correlation method (Cea et al. (2007)).

The second device was a Yaw type Preston tube for local bed shear stress measurement. This instrument was manufactured using 3 brass tubes with external diameters of 3.1 mm. The face of the middle tube was completely flat and the side tubes were chamfered at an angle of 45 degree. The manufactured probe was connected to three capacitive types, Keller 41X pressure transducers using silicon tubing. The accuracy and sampling rate of transducers were 0.1% of full scale and 100 Hz respectively. A special method was used to calibrate the pressure transducers and the zero point of all of them was set to the hydrostatic pressure of the undisturbed approaching flow to improve the accuracy of the output signals by decreasing the reading pressure range. Finally the raw data (i.e. pressure differences) were processed to obtain bed shear stresses using the calibration method proposed by Rajaratnam & Muralidhar (1968). The yaw probe was connected to a point gauge with an instrument rail bearing system that can be moved precisely along the flume and in lateral and vertical directions. The control of traversing system, data logging and processing of ADV and Yaw probe recorded time series accomplished with integrated software developed using the LabVIEW programming.

#### 3.3 Experimental program and procedure

Preliminary experiments were conducted to investigate the development of the free stream turbulent flow along the flume using ADV. Purposes of this measurement were: (1) to determine the developing length of the turbulent boundary layer. The mean bed shear stress in the developed section will be used to normalization shear stress in the main experiments; (2) verification of the velocity profile measured with the manufactured Yaw probe in the fully developed section of the uniform flow.

The water discharge was 60 lit/s and the equivalent normal depth  $h=143\text{mm}$  was applied in the flume entrance by adjusting the end flap weir. Water surface profile was measured with the point gauge and the flow uniformity was confirmed by comparing the channel bed slope with surface profile. Seven longitudinal velocity profiles in the vertical direction were measured along the center line of the flume at intervals of 1m and at each section velocity profile were measured at 18 points with non-uniform spacing from 1mm near the bed to 15 mm near the water surface. The sampling frequency of the ADV was set to 100 Hz

and at each measuring node, 18000 instantaneous velocities (i.e. 3 min measurement) were recorded. Time series were filtered using the velocity correlation method (Cea et al. (2007)) and time averaged flow velocity profiles are illustrated in Fig. 3. By examining velocity profiles in this figure, it can be seen that flow is fully developed when  $x \geq 7m$ . In main experiments groynes will be installed in the fully developed region. Yaw probe measurements for velocity distribution are also compared with ADV results at a section in the fully developed region with very good agreement (Figure 3b). In the next step, the lateral distribution of bed shear stress was measured in a fully developed cross section using the Yaw probe and the average bed shear stress value was found and compared with that calculated from  $\tau = \rho g R s$  and agreement was good, showing the accuracy of the Yaw probe.

Experiments were conducted to measure the local bed shear stress around single groynes with two different shapes. Geometrical definitions of tested groyne shapes are illustrated in Fig. 2.

Table 1 summarizes the conducted experiments. As indicated in Table 1, three experiments were conducted named S-D, T-H and T-F with straight groyne, T shape groyne ( $L'=0.5L$ ) and T shape groyne ( $L'=L$ ) respectively.

Groynes were made from 1 cm thick and 25 cm high Perspex plates. The origin of the X axis was assumed at the groyne position and distances were normalized with groyne main length (L). In the case of T shape groynes, the upstream tip of the groyne wing was located at  $X/L=0$ . The ratio between groynes main length and the channel width is  $L/b=0.15$ , where the b is the channel width. The Ratio between the length and the height of the groynes ( $b/h$ ) was equal to 1.05. From application point of view this corresponds to short groynes.

The groynes did not submerge in any of the experiments.

Fig. 4 illustrates measurement grids for all three types of groynes. The measurement domain extended  $4L$  upstream and  $9L$  downstream of the groyne location. The domain width was  $4L$ . Thirty one cross sections with non uniform spacing, including 8 upstream of the groyne, one at the groyne tip (upstream tip of the wing in the T shape case) and 22 downstream of the groyne were measured in each experiment. Each cross section contains 21 points and they were clustered around the groyne tip (in front of the wing in T shape groyne) and along the wake zone.

It was not possible to measure the bed shear stress adjacent to the groyne tip and also along the upstream face of the groyne due to yaw probe dimension. In these cases a two tube instrument (standard Preston tube) was used for shear stress measurement. The dynamic port of the probe was positioned at the measuring point and aligned with the local flow direction found by dye injection tests.

An investigation was carried out to define the sampling time needed for determination of mean shear stress at each measuring point. The developed software for data logging and data processing was able to calculate and plot simultaneously the average of the measured shear stress time series. This average should not change by time in a steady state flow.

Table 1. Summary of experimental conditions.

Experiment ID	L (m)	L' (m)	U <sub>app</sub> (m/s)	Fr (-)	Re (-)
S-D	0.15	0.000	0.42	0.35	60000
T-H		0.075			
T-F		0.150			

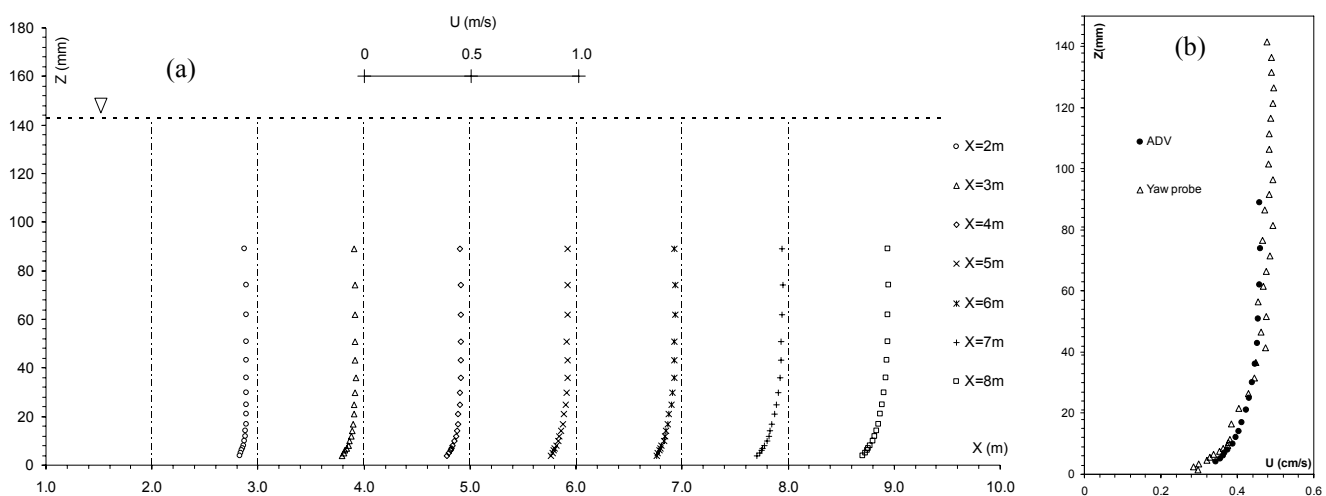


Figure 3. Flow development along the flume and comparison of vertical velocity profiles in the fully developed section.

So at each point this criterion has been used to control the sampling time needed to provide converged statistics of the mean shear stress.

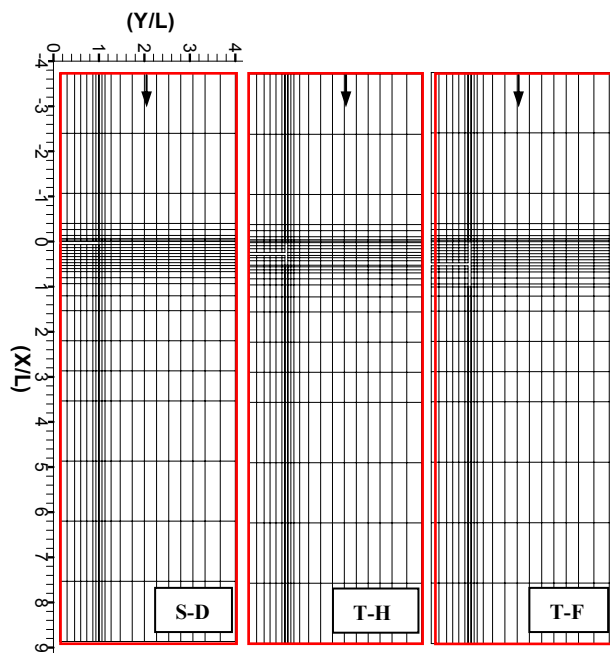


Figure 4. Measuring domains and grids.

#### 4 RESULTS AND DISCUSSION

Bed shear stresses measured in different experiments are presented in Fig. 5. The shear amplification ( $\tau/\tau_{00}$ ) in the contour plots relate the local shear stress at any position,  $\tau$ , to undisturbed fully developed uniform flow mean shear stress,  $\tau_{00}$ . The dashed lines marked regions around the groynes tip are enlarged and presented in more details.

These plots indicate in general: 1) the effect of groyne on the flow field and consequently on the bed shear stress is already detectable at  $X/L=-4$ . The bed shear stress near the right wall is lower than  $\tau_{00}$  and increases towards the channel center, 2) considerable increase in bed shear stress occurs around the tip and immediate neighborhood of groynes. The largest bed shear amplification values are around the tip (near the up stream tip in T shape groynes) but high bed shear stress values also extends towards downstream, (3) The total shear stress in the vicinity of the groyne is a combination of shear stress due to contraction (contraction amplification) and shear stress due to the diversion of the streamlines due to the presence of the groyne structure and its accompanied vortex system (local amplification).

For the straight groyne, because of the back-water effect, approaching flow progressively decelerates along the right wall and consequently, bed shear reduces towards the upstream face of

the groyne. On the other hand, visualizations showed that the near bed reversed flow at the upstream face of the groyne, acts as a jet like flow and interaction of the approach flow and the jet flow, cause the formation of the horseshoe vortex (HV) around the base of the groyne. The HV system lies near the side wall, parallel to the upstream face of the groyne (the core of the vortex is approximately at  $X/L=-0.2$ ), and changes its orientation until to being parallel to the SL at the tip of the groyne.

Fig. (5d) illustrates the enlarged details of the distribution of the bed shear in the vicinity of the straight groyne. It can be seen that the bed shear stress is amplified in the region beneath the HV system along the  $Z/L=-0.2$  line.

Visualization showed flow accelerates strongly first in lateral direction, starting from mid length of the groyne toward groyne tip and at the groyne tip it accelerates tangential to the SL. Fig. 6 illustrates these phenomena. This phenomena affect the bed shear stress and the largest values of shear amplification ( $\tau/\tau_{00}=4.3$ ) occurs around the groyne tip. This is consistent with experimental observations of Radice et al. (2006) that showed scour is initiated in the groyne tip region. Due to the flow acceleration the high shear region extends also laterally along the upstream face of the groyne in a limited thin zone.

Contraction shear amplification is detectable up to  $X/L=-3$  upstream of the groyne and its effects are present until a long distance downstream of the groyne.

Interaction of the recirculating flow downstream of the groyne, separated shear and the down stream extension of the horseshoe vortex and its interaction with the shear layer and also flow contraction result in a very complex flow structure downstream of the groyne.

Above mentioned flow mechanisms directly affect the distribution of bed shear stress and among them, the horseshoe vortex and the separated shear layer have more significant contribution in local shear amplification. The most interesting feature of the shear map at the downstream of the straight groyne is development and extension of the higher bed shear zone.

As shown in Fig. 5, in T shape groyne, the maximum amplification is smaller than the straight groyne. It does not occur at groyne tip and shifts toward the channel center. Furthermore, the high shear region after the upstream tip of the groyne is confined to a smaller area and is decaying much faster toward down stream.

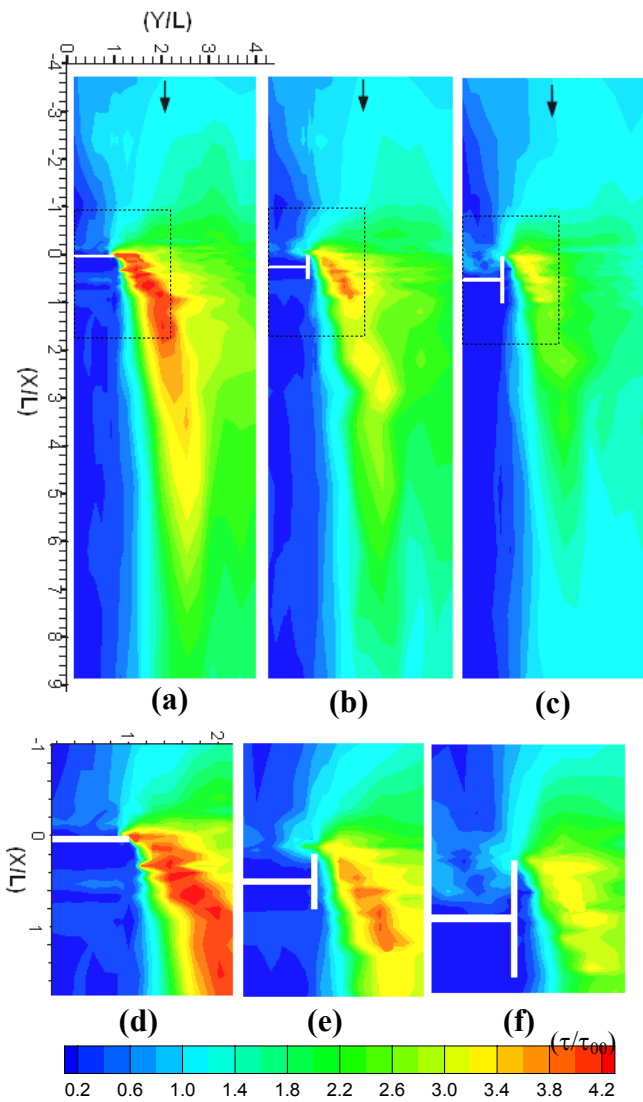


Figure 5. Shear stress amplification contours.



Figure 6. Flow visualization at the tip of straight groyne.

Shear stress distribution at the upstream part of the T shape groynes is also different from the straight groyne. There are two distinct high shear zones, one around the upstream tip of the wing and shear amplification is also detectable near the intersection of groyne and the right wall.

Fig. 7 illustrates the comparison of bed shear profiles along the cross section passing from upstream face of the straight groyne and upstream tip of the T shape groynes ( $X/L=0$  line).

In this figure local amplification of the bed shear stress near the right wall, especially for TF groyne, is obvious. The most important feature of this figure is the distinct difference between maximum amplification of bed shear for the two types. In straight groyne as mentioned before, the shear amplifies in order of 4.3 but for T shape groynes the maximum amplification factors for TH and TF types are 3.5 and 2.9 respectively which shows that the shear intensity reduces about 35% in TF case in comparison to straight groyne. Furthermore the maximum shear amplification occurs at  $Y/L=1$  for straight groyne, but in T shape groynes the high shear zone shifts toward the channel center.

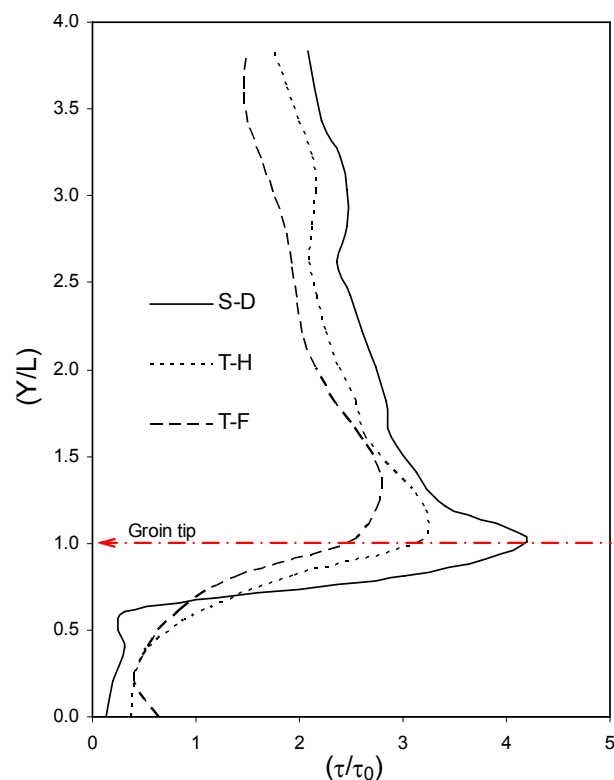


Figure 7. Lateral distribution of Bed shear profiles at ( $X/L=0$ ) cross section.

A small but relatively strong vortex is present at the intersection between the upstream face of the T shape groyne and the right wall. This vortex is intensified in TF groyne relative to TH case. Visualizations showed that the corner vortex has a tornado like structure over the channel depth and its size is reduced from water surface toward the channel bed. This vortical flow structure affects the distribution of the bed shear stress and the local amplification of the bed shear near the right wall (see Fig. 7).

## 5 SUMMARY AND CONCLUSIONS

Distribution of bed shear stress around single groyne with straight and T shape plan views at high Reynolds number ( $Re=60000$ ) were measured and investigated experimentally. It was found that the maximum bed shear amplification in the T shape groyne is 35% less than the straight one. It does not occur at groyne tip and shifts toward the channel center. Furthermore the high shear region after the upstream tip of the groyne is confined to a smaller region and is more uniform than straight groyne. Consequently it is expected that in movable bed condition the depth of the local scour be less than the straight groyne.

## REFERENCES

- Ahmed, F., Rajaratnam, N. 2000. Observations on flow around bridge abutments. *J. Eng. Mech., ASCE*, 126(1),51-59.
- Awazu, S. 1967. On scour around spur dike. Proc., 12th Congr. Of the IAHR, Delft, The Netherlands.
- Basak, N.,N., 1999. Irrigation Engineering. McGraw-Hill.
- Cea, L., Puertas, J., and Pena, L. 2007. Velocity measurements on highly turbulent free surface flow using ADV. *Exp Fluids*, 42(3), 333-348.
- Domboroski, D., Crimaldi, J. 2007. The accuracy of acoustic Doppler velocimetry measurements in turbulent boundary layer flows over a smooth bed. *Limnol. Oceanogr. Methods*, 5, 23-33.
- Dey, S., and Barbhuiya, A. 2005. Turbulent flow field in a scour hole at a semicircular abutment. *Can. J. Civ. Eng.*, 32(1),213-232.
- Duan, J., 2009. Mean flow and turbulence around a laboratory spur dike. *J. Hydraul. Eng.*, 135(10),803-811.
- Duan, J., He, L., Fu, X., Wang, Q. 2009. Mean flow and turbulence around a experimental spur dike. *Adv. Water Resour.* 132(12), 1717-1725.
- Fazli, M., Ghodsian, M., and Salehi Neyshaboury, S.A.A. 2008. Scour and flow field around a spur dike in a 90° bend. *International Journal of Sediment Research*, 23(1),56-68.
- Molinas, A., Kheireldin, K. and Baosheng, W. 1998. Shear stress around vertical wall abutments. *J. Hydraul. Eng.*, 124(8), 822-830.
- Paik, J., and Sotiropoulos, F.2005. Coherent structure dynamics upstream of a long rectangular block at the side of a large aspect ratio channel. *J. Phys. Fluids.*, 17(11), 115104-115104-14.
- Precht, E., Janssen, F., and Huettel, M. 2006. Near-bottom performance of the acoustic Doppler velocimeter (ADV)-a comparative study. *Aquatic Ecology*, 40, 481-492.
- Radice, A., Malavasi, S., and Ballio, F. Sediment kinematics in abutment scour. *J. Hydraul. Eng.*, 134(2),146-156.
- Rajaratnam, N., and Muralidhar, D. 1968. Yaw probe used as preston tube. Technical Note, Aero J., Roy. Aero. SOC. 72, 1059-60.
- Rajaratnam, N., Nwachukwu, B. 1983. Flow near groin-like structures. *J. Hydraul. Eng.*, 463-480.
- Teruzzi, A., Ballio, F. and Armenio, V. 2009. Turbulent stresses at the bottom surface near an abutment: laboratory-scale numerical experiment. *J. Hydraul. Eng.*, 135(2),106-117.
- Tingsanchali, T., Maheswaran, S. 1990. 2-D depth averaged flow computation near groyne. *J. Hydraul. Eng.*, 116(1), 71-86.
- Vaghefi, M., Ghodsian, M. Experimental study on scour and flow field in a scour hole around a T-shape spur dike in a 90° bend. 2008. *International Journal of Sediment Research*, 24(2),145-158.
- Zaghloul, N. A. 1974. Analytical and experimental investigation of flow around a spur dike. PhD dissertation, Civ. Engrg. Dep., University of Windsor, Windsor, Ontario, Canada.